LANGMUIR

pubs.acs.org/Langmuir Article

A Sub-Micron Spherical Atomic Force Microscopic Tip for Surface Measurements

Huan Hu,* Bin Shi, Christopher M. Breslin, Lynne Gignac, and Yitian Peng*

Cite This: *Langmuir* 2020, 36, 7861−7867 Read Online

ACCESS | Metrics & More | Article Recommendations | Supporting Information

ABSTRACT: We report a novel methodology for fabricating a sub-micron spherical atomic force microscope (AFM) tip controllably—a silicon sub-micron sphere atop microcantilevers, which is desired for precise nanoscale tribology measurements, biological studies, and colloid science. Silicon sub-micron spheres are fabricated through swelling of single-crystal silicon with proper high-energy helium ion dosing, a traditionally undesired phenomenon known in helium ion microscopy. Silicon sub-micron spheres with diameters from 100 nm to 1 μm are demonstrated, and the placement of silicon sub-micron spheres can be as accurate as 10 nm or even below. This AFM tip demonstrates robust measurements during friction tests on graphene/silicon oxide substrates for more than 10 000 cycles. This AFM tip overcomes a critical challenge of reducing the size of spherical AFM tips from the micrometer scale to the sub-micron scale and is promising in cross-scale mechanics studies, nanotribology, colloid science, and biology.

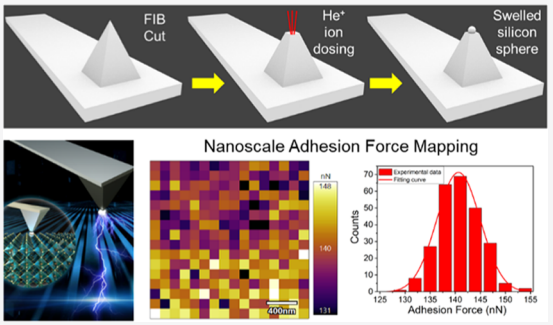

INTRODUCTION

Spherical atomic force microscopic (AFM) or colloidal AFM tip, referring to a microcantilever with a rounded tip instead of a sharp tip, has very promising applications in colloidal force measurements,[1] biological force measurements,[2] nanoscale adhesion on textured surfaces,[3] nanomanipulation,[4] AFM-based force spectroscopy,[2] and scanning probe nanolithography.[5] For example, a rounded tip can prevent local rupture of either the cell membrane in biological studies[6] or a thin suspended membrane[7] during a mechanical test, therefore providing more reliable and safer measurements. Emerging applications such as near-field scanning optical microscopy (NSOM) and tip-enhanced Raman scattering (TERS) pose unique fabrication challenges, such as accurate placement of sub-micrometer particles on a tip.[8] The current fabrication strategies of spherical AFM tips are not ideal and lack precise placement, good control of spherical shape, and strong adhesion between the sphere and cantilevers.[8−11] In this paper, we present a new methodology for preparing sub-micron spherical AFM tips with controlled diameters from 100 nm to 1 μm based on the observed phenomenon that helium ions can swell single-crystal silicon substrates.[12] We demonstrate precise control of amorphous silicon sub-micron spheres with diameters from 100 nm to 1 μm by controlling the dose from 10 000 ions/nm^2 to 40 000 ions/nm^2. Precise placement of spheres with lateral resolution as small as 10 nm is demonstrated and can be further improved if necessary.

An ideal colloidal AFM tip should satisfy three criteria. First, the tip shape needs to be as close to spherical as possible; second, the sphere should be placed right on the center of a microcantilever to avoid undesired twisting during a force test; third, the spheres and cantilevers should bind firmly to avoid failure. Existing preparation methods can be categorized into two types: the first type is to attach microspheres onto tips,[13−15] which is a process lacking repeatability and reliability. Moreover, the lateral placement resolution is limited to the micrometer scale. The other type is to modify the tip geometry through thermal oxidation,[16] material deposition,[17,18] etching,[19] rounded cavity molding,[9] aspiration of nanospheres,[20] etc. No existing methods for preparing spherical AFM tips can meet the three criteria simultaneously.

A helium ion microscope (HIM), a relatively new instrument with an atomic-size source providing sub-nanometer-resolution helium ion beams,[21] has been applied in various applications, including biological imaging,[22] nanolithography with sub-10 nm features,[23−25] milling metals and two-dimensional (2-D) materials[26] with sub-5 nm resolution, creating superconducting tunneling junctions,[27] drilling nanopores,[28,29] and three-dimensional (3-D) nanoscale lithography.[30] However, helium ions can implant into substrates such as single-crystal silicon and cause severe swelling sometimes termed "ballooning" above the threshold of 13 000 ions/nm^2.[12]

Received: April 1, 2020
Revised: June 8, 2020
Published: June 9, 2020

https://dx.doi.org/10.1021/acs.langmuir.0c00923
Langmuir 2020, 36, 7861−7867

This swelling phenomenon is typically undesired and can be reduced by laser-assisted processing.[31] Here, we took advantage of this typically undesired phenomenon and employed it in fabricating sub-micron spherical AFM tips with precisely defined spherical diameters and at precisely defined locations on a microcantilever. Moreover, the spheres and the cantilever are integral parts and can therefore withstand large force, thus ensuring repeatability and reliability. Our technology satisfies all of the criteria for an ideal colloidal probe.

EXPERIMENTAL SECTION

Fabrication Process of Sub-Micron Spherical Probes. Figure 1a shows the procedures for fabricating a sub-micron spherical AFM tip. A commercial AFM probe [Bruker TESP-V2] was mounted on edge, incident to an ion beam. A FEI Helios 400 DualBeam was used, with a 300 pA 30 kV Ga+ beam, to remove the top ~2 μm from the AFM tip. This step creates a flat plateau for the swelled silicon sphere to form. After flat plateau creation, 30 keV helium ions are implanted into a 300 nm diameter circle, with a dose of 20 000 ions/nm^2, as shown in Figure 1a. The swelled silicon forms a sphere with ~500 nm diameter. Figure 1b–d shows the scanning electron microscopy (SEM) image of the swelled silicon sphere on the flat plateau with 2000, 5000, and 50 000 magnifications.

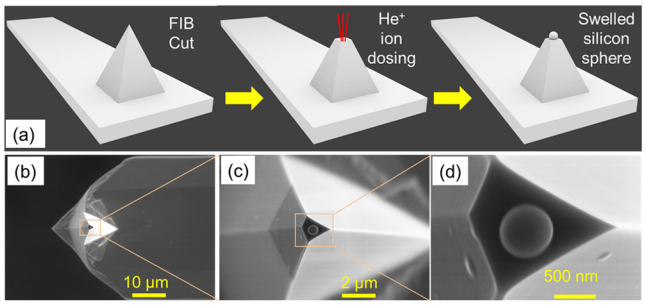

Figure 1. (a) Schematic showing the process of making a colloidal AFM using a focused ion beam (FIB) and a helium ion microscope (HIM). SEM images of a swelled silicon sphere formed on the plateau after helium ion dosing (b) with 2000 magnification, (c) with 5000 magnification, and (d) with 50 000 magnification.

The helium ion microscope has an atomic resolution tip consisting of three atoms called a trimer that can ionize helium gas in a high electrical voltage bias. The helium ions are then accelerated and go through a series of apertures and beam lenses and finally focus on an illuminating circular spot with a diameter of less than 0.5 nm. When fabricating the sub-micron sphere, we first programmed the dosing area consisting of an array of spots with controlled spacing. Then, we controlled the focused helium ion beam to dwell at each spot for a programmed duration and move to the next spot till all of the spots were dosed. The spot spacing and the dwelling time can be controlled. Given a specific focused helium ion beam current of normally around 1 pA, the corresponding dose of this circle is set to 15 000 ions/nm^2, and less than 1 min is required to fabricate a 300 nm diameter silicon sphere.

This approach has several advantages. First, the diameter of the swelled silicon sphere can be controlled precisely by adjusting helium ion doses. Figure 2 shows silicon sub-micron spheres with increasing diameter from 270 to 510 nm prepared with increasing helium ion dose from 10 000 to 50 000 ions/nm^2. The diameter of dosed circles is held constant at 250 nm. The inset SEM images show the swelled silicon spheres with the same 70 000 magnification. The scale bar is 500 nm. To make a good sphere, a proper dose is important. Starting from 30 000 ions/nm^2, we observed damage on the surface, resulting in spheres with a big hole on the top due to ion damage. Spheres of diameters from 100 to 1000 nm were also prepared, as shown in Figure S4 in the Supporting Information, by changing the dosing areas.

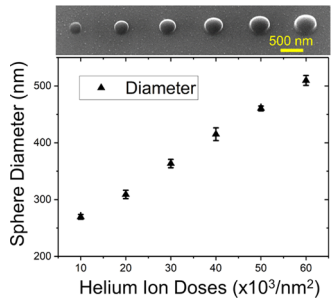

Figure 2. Size study of swelled silicon. Diameters of the swelled silicon sub-micron spheres at different helium ion doses from 10 000 to 60 000 ion/nm^2. A helium ion beam of 30 kV and 2.7 pA was used. Each dosing area is a 250 nm diameter circle. The top inset figure is a tilted-view scanning helium ion microscopic image of six swelled silicon sub-micron spheres.

Second, the positions of the silicon sub-micron spheres can be precisely controlled with lateral resolution as small as 10 nm, an equipment-imposed limit. Under ideal conditions, such as less environmental noise and sample drift, sub-10 nm spacing can be achieved. This makes it suitable for fabricating colloidal AFM tips with precisely positioned sub-micron spheres. Figure 3a shows three different sizes of silicon sub-micron spheres formed using the same doses but different sizes of circles.

Figure 3b shows a 30° tilted view of scanning helium ion microscopic image of IBM logo formed by identical silicon spheres. The silicon spheres have a diameter of 400 nm and are spaced by approximately 60 nm. Figure 3c shows a top-down scanning helium

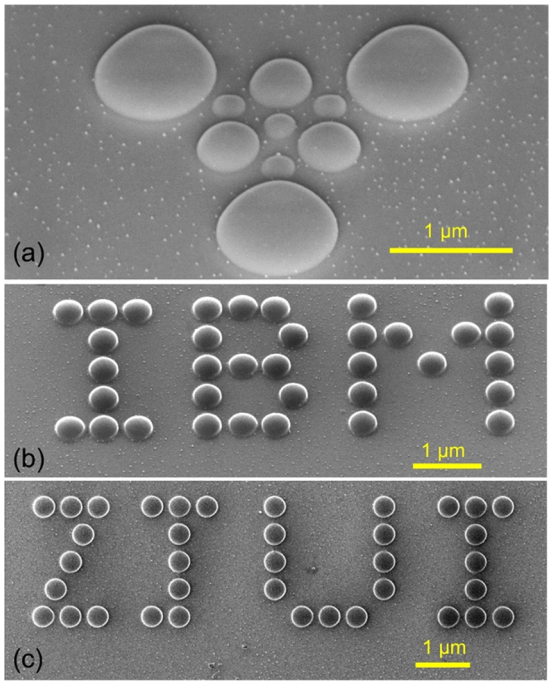

Figure 3. (a) Tilted-view (45°) scanning electron microscopic image of three different sizes of swelled silicon spheres aligned in a coordinated form. (b) Tilted-view (30°) scanning helium ion microscopic image of aligned swelled silicon sub-micron spheres forming an IBM logo; each swelled silicon sphere is about 400 nm spaced by 50 nm. (c) Top-view scanning helium ion microscopic image of aligned swelled silicon sub-micron spheres forming a ZJUI logo; each swelled silicon sphere is about 400 nm spaced by 100 nm.

https://dx.doi.org/10.1021/acs.langmuir.0c00923
Langmuir 2020, 36, 7861−7867

ion microscopic image of "ZJUI" logo, also formed by identical silicon spheres. The silicon spheres have a diameter of 400 nm and are spaced by approximately 100 nm. All three figures show the capability of our technology in precisely controlling the sphere sizes and locations.

It is also important to investigate the properties of the swelled silicon. Six identical regions with 250 nm × 2 μm rectangles were irradiated with 30 keV He^+ ions using a dose from 522 ions/nm^2 (1×) to 2×, 5×, 10×, 20×, and 40×. The current of the He^+ ions used was 5.36 pA with a 10 μm aperture and a spot size of 3. After irradiation, an x-section transmission electron microscopy (TEM) sample was prepared using a focused ion beam (FIB) machine—in situ electron beam-induced platinum deposition over features is done first to protect the surface from gallium ion beam damage. TEM (300 kV) was used to image the sample, and the results are shown in Figure 4.

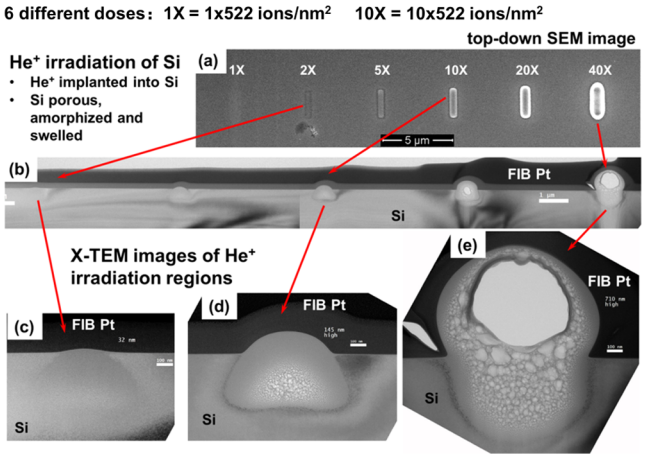

Figure 4. Studies of the He^+ irradiation of silicon: (a) top-down SEM image of six equally shaped regions (250 nm × 2 μm) but with varying doses (scale bar 5 μm); (b) cross-sectional SEM image of the six regions post FIB x-section (scale bar 1 μm); and (c–e) X-TEM image of He^+-irradiated region using doses of (c) 1044 ions/nm^2, (d) 5220 ions/nm^2, and (e) 20 880 ions/nm^2 (scale bars 100 nm).

The results show that the irradiated silicon starts to show swelling at around 1044 ions/nm^2 dose. And the silicon becomes more porous and nanoscale bubbles are formed at around 5220 ions/nm^2. With increased He^+ dosing, bigger bubbles appear and eventually turn into microscale bubbles at a dose of 20 880 ions/nm^2. This observation agrees well with reported studies.[32,33] The significance of swelling cannot be overstated—the unique 3-D shape is difficult for conventional semiconductor manufacturing technology to produce and is highly desired for colloidal AFM and NSOM tips. Adding to the versatility, spherical tips can be coated with different types of materials for testing.

Depending on the size of the sub-micron sphere, it takes from several seconds to several minutes to fabricate the sub-micron spheres. The two determining factors of preparation time are the dose intensity and the dose area. The success rate can be 100% as long as the helium ion microscope is working properly, which means that the high-energy helium ion beams can be focused onto a spot with less than 0.5 nm diameter and the beam movement path can be controlled precisely.

Procedures for Graphene Imaging and Adhesion Force and Friction Measurements. Graphene was mechanically exfoliated from highly oriented pyrolytic graphite (HOPG, XFNANO Inc.) and deposited onto a Si substrate with a 300 nm thick insulating silicon oxide.[34] The thickness of graphene was initially identified by optical microscopy followed by measurements using AFM (MFP-3D, Asylum Research Inc.). The spring constant and resonance frequency of the probe with a spherical colloidal tip are 42 N/m and 320 kHz, respectively. Nanotribological properties of graphene were studied by measuring the friction force as a function of normal force under ambient conditions (20–30 °C and 30–40% RH). The normal force was calibrated using a noncontact method.[35] The adhesion force was determined by measuring the pull-off force, which was the maximum force to pull the AFM tip out of contact with the surface. The normal force used for the adhesion force measurement was 10 nN and the loading rate was 1 Hz. Friction tests were performed by obtaining the friction loops in an area of 1000 × 1000 nm with a scanning speed of 2.5 μm/s. Each friction loop corresponds to a complete trace and retrace scan over the same line, and the friction is equal to half the difference between the lateral forces obtained through trace and retrace scanning. The quantitative friction was based on the average values measured through repeating the friction test 3 times.

Procedures of Electrochemical Scanning Probe Lithography. Graphene was mechanically exfoliated from a highly oriented pyrolytic graphite sample (HOPG, XFNANO Inc.) and deposited onto a conductive substrate. The substrate was prepared by evaporating a 5 nm thick Cr film and a 95 nm thick Au film on a silicon substrate with a 300 nm thick SiO_2 film. The graphene was initially identified by optical microscopy, followed by measurements using AFM (MFP-3D, Asylum Research Inc.). The nanopatterns on graphene were fabricated using AFM-based electrochemical functionalization. During nanopatterning, a constant bias voltage of −4 V was applied to a conductive AFM probe with a 25 nm Pt/Ir coating (EFM, Nanoworld Inc.). Then, the tip moved along a given path at a speed of 500 nm/s. The experiments were performed under ambient conditions (27 ± 1 °C and 53 ± 2% relative humidity). The normal force constant of the AFM probe was calibrated using a noncontact method.

RESULTS AND DISCUSSION

Application of the Sub-Micron Spherical AFM Tip for Imaging and Adhesion and Friction Measurements. First, we employed the sub-micron spherical AFM tip for imaging a graphene sample (sample preparation procedures are provided in the Supporting Information). For comparison, we also used a commercial AFM probe (Multi-75Al-G, Budget sensors) with a sharp tip to scan the same sample in AC mode (estimated radius 10 nm, resonance frequency = 75 kHz, spring constant K_c = 3.0 N/m) to measure the topographic image. Figure 5a,b shows the schematic description of the scanning experiments. Figure 5c shows the topographic image measured by the sub-micron spherical AFM tip using the AC mode. Figure 5d shows the results measured by the sub-micron spherical AFM tip using the contact mode. The thickness of monolayer graphene measured by the sub-micron spherical AFM tip in AC mode and DC mode (contact mode) are 1.9 and 0.9 nm (Figure 5f,g), respectively. Figure 5e shows the topographic image obtained by the commercial AFM tip. The measured height of the monolayer graphene is 0.6 nm, as shown in Figure 5h. The theoretical thickness of single-layer graphene is reported to be 0.35 ± 0.01 nm [3]. The measured thickness of single-layer graphene on a SiO_2 substrate is reported to be in the range of 0.4–1.7 nm.[36] The difference between the theoretical thickness and measured thickness is attributed to the instrumental offset that is caused by the tip–substrate interactions, surface chemistry, and imaging feedback settings.[36] Our sub-micron spherical AFM tip can obtain clear images in AC mode with a single layer of graphene, which is very advantageous to obtain the sample morphology and confirm the position precisely. This is very convenient and beneficial for further measurements such as adhesion force mapping and friction measurements.

Second, we employed the sub-micron spherical AFM tip to measure the adhesion force between silicon and graphene. The adhesion force was determined by measuring the pull-off force, which was the maximum force to pull the AFM tip out of

https://dx.doi.org/10.1021/acs.langmuir.0c00923
Langmuir 2020, 36, 7861–7867

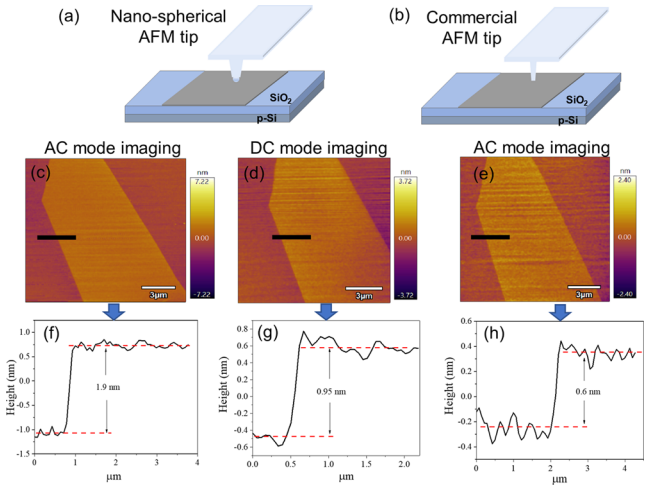

Figure 5. (a) Schematic drawing showing sample measurement by the sub-micron spherical AFM tip. (b) Schematic drawing showing sample measurement by the commercial AFM tip. (c) AFM topography image obtained by the sub-micron spherical AFM tip in AC mode imaging. (d) AFM topography image obtained by the sub-micron spherical AFM tip in DC mode imaging. (e) AFM topography image obtained by the commercial AFM tip in AC mode imaging. (f) Thickness of the graphene monolayer measured by the sub-micron spherical AFM tip in AC mode is 1.9 nm. (g) Thickness of the graphene monolayer measured by the sub-micron spherical AFM tip in DC mode is 0.95 nm. (h) Thickness of the graphene monolayer measured by the commercial AFM tip in AC mode is 0.6 nm. All measurements were performed on the same monolayer graphene exfoliated on a p-doped silicon substrate with a 300 nm thick SiO_2 layer.

contact with the surface. The normal force used for adhesion force measurements was 100 nN and the loading rate was 1 Hz. Figure 6a,b shows the adhesive force map with 256 points

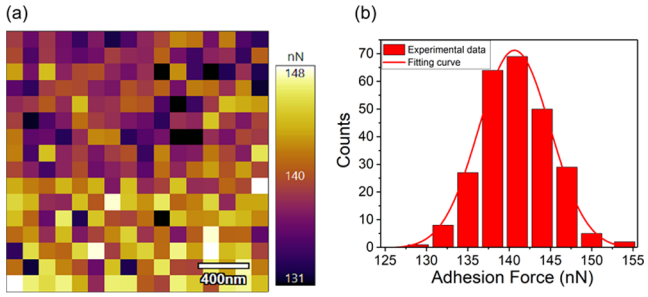

Figure 6. (a) Adhesion force map of the surface area obtained using the sub-micron spherical AFM tip. (b) Statistical analysis histograms of adhesion forces on monolayer graphene.

on a monolayer graphene film and the results of the Gaussian statistical analysis, respectively. It is found that the adhesive force is between 126.1 and 153.3 nN and the adhesive forces obey the Gaussian distribution well. The adhesion force map measurement shows that the adhesion forces on the bottom area are slightly higher than that on the upper area. The reason can be attributed to two factors. First, the scan was from top to bottom and the slight wear of the spherical tip developed during the scan might cause the increase of adhesion forces. Second, the mapping of the adhesion force was obtained by scanning in the top to bottom direction. The graphene might undergo strong puckering to increase the area during scanning.

Third, we performed the friction measurement using the sub-micron spherical AFM tip. Figure 7a shows the friction

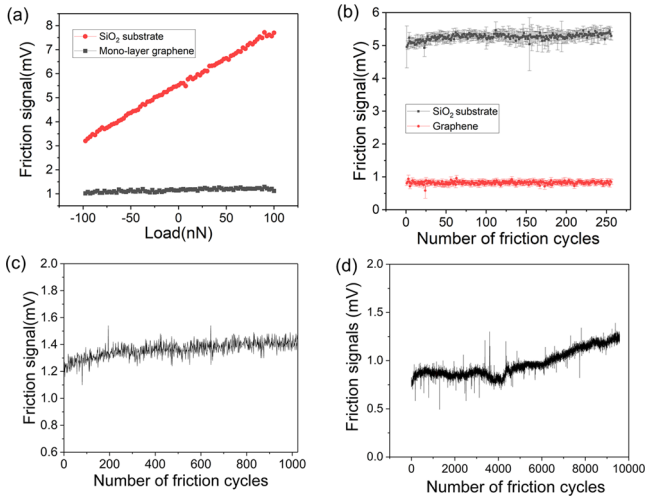

Figure 7. (a) Comparison of friction forces as a function of normal force on the graphene and on the SiO_2 substrate. (b) Friction on the graphene and on the SiO_2 substrate versus friction cycles. (c) Friction on graphene versus the number of friction cycles (up to 1000 cycles). (d) Friction on graphene versus the number of friction cycles (up to 10 000 cycles).

force measured on the graphene and on the SiO_2 substrate with applied loading forces ranging from −100 to 100 nN. The friction of the SiO_2 substrate decreases significantly with the decrease of normal load. However, the friction of graphene varies little with the applied load because of the lower friction. The difference between the friction force on graphene and on the substrate can be used to determine whether the graphene is worn out by the AFM tip. To test the reliability and robustness of the spherical AFM tip, we performed the friction measurement at a constant applied load of 10 nN and repeated it 256, 1000, and 10 000 times. Figure 7b shows the measurement of 256 reciprocating cycles for both SiO_2 substrate and graphene substrate. The measurement clearly shows that graphene can steadily reduce the friction of the SiO_2 substrate by more than 5 times, which is significant and consistent with existing reports. Figure 7c,d shows the friction measurement on graphene for 1000 and 10 000 reciprocating cycles. No significant increase of friction on graphene was observed, which means the graphene was not removed by the tip over 10 000 friction scans, showcasing the reliability of our sub-micron spherical AFM tip. The small increase in friction after 4000 cycles in Figure 7d is likely to be caused by the sphere wear accumulated during the friction test, as shown in Figure S6a.

The morphology of graphene before and after 10 000 friction tests were scanned by the sub-micron spherical AFM tip, as shown in Figure S2a. No wear of graphene was observed after 10 000 cycles of friction test. The adhesion between the sub-micron spherical AFM tip and graphene was also measured before and after 10 000 friction tests. The adhesion did not show significant changes before and after 10 000 cycles of friction test. Both the morphology test and adhesion measurement denote the robust mechanical and adhesive properties of our fabricated sub-micron spherical AFM tip for nanofriction experiments.

https://dx.doi.org/10.1021/acs.langmuir.0c00923
Langmuir 2020, 36, 7861−7867

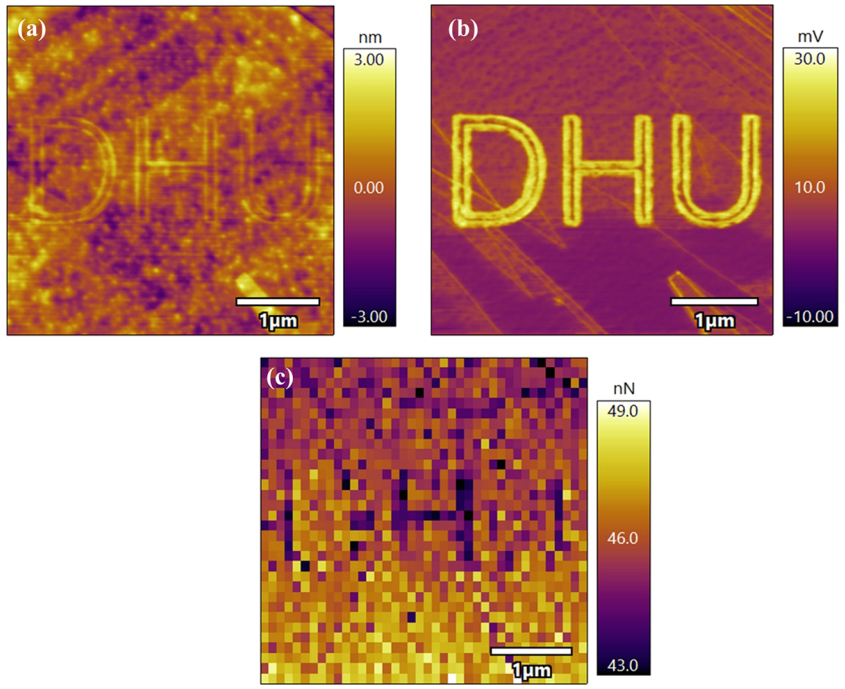

Figure 8. (a) Topography image of the nanopatterned graphene sample obtained using the sub-micron spherical AFM tip in AC imaging mode. (b) Friction map and (c) adhesion force map of the DHU-patterned monolayer graphene produced by anodic oxidation of a commercial conductive AFM tip. All images are obtained by the sub-micron spherical AFM tip.

Finally, we designed an experiment to showcase the potential of our sub-micron spherical AFM tip. We first fabricated nanometer scale "DHU" patterns on a graphene sample using a commercial conductive AFM tip via electrochemical scanning probe lithography (fabrication procedure is explained in the Supporting Information). Then, we employed our sub-micron spherical AFM tip to do measurements. The topography and friction of patterned graphene were measured by a 300 nm diameter sub-micron spherical AFM tip in contact mode under a normal load of 10 nN. Figure 8a,b shows the topography image and friction image of graphene, respectively, with patterned letters of DHU. The DHU patterns are taller and have larger friction because of the electrochemical functionalization. Since our sub-micron spherical AFM tip has relatively small dimensions, the nanopatterns can be easily identified, which is not possible with a microspherical AFM tip. After obtaining clear images of nanopatterns, we further performed adhesion force mapping with good precision. Figure 8c shows the adhesion mapping, and the DHU nanopatterns can be identified, although not very clearly. The roughness of the substrate led to a large fluctuation of adhesive force, which made the pattern a bit vague.

Our method is a significant step forward in the technology development of spherical AFM tips in three aspects. First, it provides improved spatial resolution for force mapping in AFM-based force spectroscopy, which is preferred in measuring smaller and smaller objects such as cells, bacteria, DNA, and proteins.[2] Second, it facilitates more robust measurement of friction force. Unlike a spherical AFM tip prepared by sub-micron particle attachment methods, the sub-micron sphere and the cantilever are an integral part and can therefore withstand larger force, thus offering reliable and repeatable measurements during friction tests that are essential in studying superlubricity.[37] Third, it provides a standard template for modeling of plasmonics and tip-enhanced Raman spectroscopy (TERS). This technology can realize mass production of highly reliable and uniform sub-micron spherical AFM tips. Although in this work, the plateau where the sub-micron sphere sits is prepared by a FIB, which is slow and not scalable, ideally, this structure can be mass-produced by conventional microfabrication. A silicon wafer consisting of hundreds of microcantilevers or microcantilevers with a plateau can be mass-produced with the standard MEMS fabrication technique. The helium ion dosing step can be automized inside the helium ion microscope for mass production of AFM tips as demanded by the community of colloidal AFM tips or colloidal probes.[38]

The swelled silicon sub-micron sphere consists of an amorphous silicon shell with trapped sub-micron helium gas bubbles and thus has lower elastic modulus and density.[39] Therefore, in certain applications, such as super rigid material measurements, smaller forces should be applied to avoid fracture. In addition, a major application of this sub-micron spherical AFM tip will be for soft materials such as polymers, biological tissues, cells, bacteria, etc.

CONCLUSIONS

We reported a novel method of using high-energy helium ions to fabricate sub-micron spheres precisely on top of microcantilevers for nanoscale friction measurements. Sub-micron spheres of diameters from 100 nm to 1 μm can be readily fabricated by adjusting the helium ion dosing area and amount. Both the shape and position of the sub-micron sphere was successfully configured with unprecedented precision compared with previous fabrication methods of spherical probes. We showed that the sub-micron spherical AFM tip can provide robust measurements up to 10 000 cycles without failure. Moreover, the nanoscale feature of this tip provides accurate imaging and meanwhile offers adhesion force mapping with nanometer precision. This sub-micron spherical AFM tip has

https://dx.doi.org/10.1021/acs.langmuir.0c00923
Langmuir 2020, 36, 7861−7867

promising applications in nanotribology, AFM-based force spectroscopy, colloidal force studies, and TERS.

■ ASSOCIATED CONTENT

Supporting Information

The Supporting Information is available free of charge at https://pubs.acs.org/doi/10.1021/acs.langmuir.0c00923.

Detailed sample preparation and experimental procedure. Adhesion force measurement details. Graphene morphology and adhesion measurement before and after 10 000 cycles of friction test. Nanopattern fabrication procedure. Spherical AFM tip with a 300 nm diameter sphere on plateaus with different sizes. Spheres fabricated using the same helium ion dose but different dose areas. Dimensions of spheres summarized. An SEM image and an optical microscopic photo of sub-microspheres after 10 000 cycles of friction test. Thickness measurement at four different sites on the monolayer graphene surface. Friction measurement on both monolayer graphene and multilayer graphene (5 nm thickness) using the sub-micron spherical AFM tip (PDF)

■ AUTHOR INFORMATION

Corresponding Authors

Huan Hu − *ZJU-UIUC Institute, International Campus and School of Information Science and Electronic Engineering, Zhejiang University, Haining 314400, China;* orcid.org/0000-0002-1317-5470; Email: huanhu@intl.zju.edu.cn

Yitian Peng − *College of Mechanical Engineering, Donghua University, Shanghai 201600, China;* orcid.org/0000-0002-4951-4657; Email: yitianpeng@dhu.edu.cn

Authors

Bin Shi − *College of Mechanical Engineering, Donghua University, Shanghai 201600, China*

Christopher M. Breslin − *IBM T. J. Watson Research Center, Yorktown Heights, New York 10598, United States*

Lynne Gignac − *IBM T. J. Watson Research Center, Yorktown Heights, New York 10598, United States*

Complete contact information is available at: https://pubs.acs.org/10.1021/acs.langmuir.0c00923

Author Contributions

H.H. initiated the concept, performed the helium ion dosing experiment, and led the whole project. B.S. conducted the tribology test. C.M.B. conducted the FIB cut of AFM tips and FIB cut of swelled silicon for TEM imaging. L.G. conducted the TEM imaging of swelled silicon at different doses. Y.P. designed and led the test of the sub-micron spherical AFM tip. H.H. and Y.P. wrote the manuscript together. C.M.B. and L.G. contributed to the manuscript revisions.

Notes

The authors declare no competing financial interest.

■ ACKNOWLEDGMENTS

This work was supported by the National Natural Science Foundation of China (Grant Nos. 61974128 and 51775105), Natural Science Foundation of Zhejiang Province (Grant No. LY19F040007), Fundamental Research Funds for the Central Universities (Grant No. 2-2050205-19-361), Natural Science Foundation of Shanghai (Grant No. 17ZR1400700), and Tang's Foundation. The work was also partially supported by Zhejiang University/University of Illinois at Urbana-Champaign Institute and led by Dr. H.H. and Dr. Y.P. The authors also thank the support of Dr. Xiaolei Wen from the University of Science and Technology of China and Jianliu Huang and Fei Zou from Zeiss.

■ REFERENCES

(1) Ducker, W. A.; Senden, T. J.; Pashley, R. M. Direct measurement of colloidal forces using an atomic force microscope. *Nature* **1991**, *353*, 239.

(2) Guo, S.; Zhu, X.; Jańczewski, D.; Lee, S. S. C.; He, T.; Teo, S. L. M.; Vancso, G. J. Measuring protein isoelectric points by AFM-based force spectroscopy using trace amounts of sample. *Nat. Nanotechnol.* **2016**, *11*, 817.

(3) Zimmermann, S.; Klauser, W.; Mead, J.; Wang, S.; Huang, H.; Fatikow, S. A laterally sensitive colloidal probe for accurately measuring nanoscale adhesion of textured surfaces. *Nano Res.* **2019**, *12*, 389−396.

(4) Shi, C. Y.; Luu, D. K.; Yang, Q. M.; Liu, J.; Chen, J.; Ru, C. H.; Xie, S. R.; Luo, J.; Ge, J.; Sun, Y. Recent advances in nanorobotic manipulation inside scanning electron microscopes. *Microsyst. Nanoeng.* **2016**, *2*, No. 16024.

(5) Garcia, R.; Knoll, A. W.; Riedo, E. Advanced scanning probe lithography. *Nat. Nanotechnol.* **2014**, *9*, 577−587.

(6) Mahaffy, R. E.; Shih, C. K.; MacKintosh, F. C.; Käs, J. Scanning Probe-Based Frequency-Dependent Microrheology of Polymer Gels and Biological Cells. *Phys. Rev. Lett.* **2000**, *85*, 880−883.

(7) Jiang, C.; Markutsya, S.; Pikus, Y.; Tsukruk, V. V. Freely suspended nanocomposite membranes as highly sensitive sensors. *Nat. Mater.* **2004**, *3*, 721−728.

(8) Gan, Y. Invited Review Article: A review of techniques for attaching micro- and nanoparticles to a probe's tip for surface force and near-field optical measurements. *Rev. Sci. Instrum.* **2007**, *78*, No. 081101.

(9) Murat Kaya, Y.; Jun, Z. Microfabrication of colloidal scanning probes with controllable tip radii of curvature. *J. Micromech. Microeng.* **2009**, *19*, No. 105021.

(10) Helfricht, N.; Mark, A.; Dorwling-Carter, L.; Zambelli, T.; Papastavrou, G. Extending the limits of direct force measurements: colloidal probes from sub-micron particles. *Nanoscale* **2017**, *9*, 9491−9501.

(11) Fan, Z.; Tao, X.; Cui, X.; Fan, X.; Zhang, X.; Dong, L. Metal-filled carbon nanotube based optical nanoantennas: bubbling, reshaping, and in situ characterization. *Nanoscale* **2012**, *4*, 5673−5679.

(12) Livengood, R.; Tan, S.; Greenzweig, Y.; Notte, J.; McVey, S. Subsurface damage from helium ions as a function of dose, beam energy, and dose rate. *J. Vac. Sci. Technol. B* **2009**, *27*, 3244−3249.

(13) Mak, L. H.; Knoll, M.; Weiner, D.; Gorschlüter, A.; Schirmeisen, A.; Fuchs, H. Reproducible attachment of micrometer sized particles to atomic force microscopy cantilevers. *Rev. Sci. Instrum.* **2006**, *77*, No. 046104.

(14) Raiteri, R.; Preuss, M.; Grattarola, M.; Butt, H.-J. Preliminary results on the electrostatic double-layer force between two surfaces with high surface potentials. *Colloids Surf., A* **1998**, *136*, 191−197.

(15) Takayuki, O.; Yamaguchi, I. Near-Field Scanning Optical Microscope Using a Gold Particle. *Jpn. J. Appl. Phys.* **1997**, *36*, L166.

(16) Hüttl, G.; Klemm, V.; Popp, R.; Simon, F.; Müller, E. Tailored colloidal AFM probes and their TEM investigation. *Surf. Interface Anal.* **2002**, *33*, 50−53.

(17) Sqalli, O.; Utke, I.; Hoffmann, P.; Marquis-Weible, F. Gold elliptical nanoantennas as probes for near field optical microscopy. *J. Appl. Phys.* **2002**, *92*, 1078−1083.

(18) Sanders, A.; Zhang, L.; Bowman, R. W.; Herrmann, L. O.; Baumberg, J. J. Facile Fabrication of Spherical Nanoparticle-Tipped AFM Probes for Plasmonic Applications. *Part. Part. Syst. Charact.* **2015**, *32*, 182−187.

(19) Ma, X.; Grüßer, M.; Schuster, R. Plasmonic nanospheres with a handle—Local electrochemical deposition of Au or Ag at the apex of optically inactive W- or C-tips. *Appl. Phys. Lett.* **2015**, *106*, No. 241103.
(20) Mark, A.; Helfricht, N.; Rauh, A.; Karg, M.; Papastavrou, G. The Next Generation of Colloidal Probes: A Universal Approach for Soft and Ultra-Small Particles. *Small* **2019**, *15*, No. 1902976.
(21) Stanford, M. G.; Lewis, B. B.; Mahady, K.; Fowlkes, J. D.; Rack, P. D. Review Article: Advanced nanoscale patterning and material synthesis with gas field helium and neon ion beams. *J. Vac. Sci. Technol. B* **2017**, *35*, No. 030802.
(22) Von Euw, S.; Zhang, Q.; Manichev, V.; Murali, N.; Gross, J.; Feldman, L. C.; Gustafsson, T.; Flach, C.; Mendelsohn, R.; Falkowski, P. G. Biological control of aragonite formation in stony corals. *Science* **2017**, *356*, 933−938.
(23) Winston, D.; Cord, B. M.; Ming, B.; Bell, D. C.; DiNatale, W. F.; Stern, L. A.; Vladar, A. E.; Postek, M. T.; Mondol, M. K.; Yang, J. K. W.; Berggren, K. K. Scanning-helium-ion-beam lithography with hydrogen silsesquioxane resist. *J. Vac. Sci. Technol. B* **2009**, *27*, 2702−2706.
(24) Li, W.-D.; Wu, W.; Williams, R. S. Combined helium ion beam and nanoimprint lithography attains 4 nm half-pitch dense patterns. *J. Vac. Sci. Technol. B* **2012**, *30*, No. 06F304.
(25) Sidorkin, V.; van Veldhoven, E.; van der Drift, E.; Alkemade, P.; Salemink, H.; Maas, D. Sub-10-nm nanolithography with a scanning helium beam. *J. Vac. Sci. Technol. B* **2009**, *27*, L18−L20.
(26) Lemme, M. C.; Bell, D. C.; Williams, J. R.; Stern, L. A.; Baugher, B. W. H.; Jarillo-Herrero, P.; Marcus, C. M. Etching of Graphene Devices with a Helium Ion Beam. *ACS Nano* **2009**, *3*, 2674−2676.
(27) Cybart, S. A.; Cho, E. Y.; Wong, T. J.; Wehlin, B. H.; Ma, M. K.; Huynh, C.; Dynes, R. C. Nano Josephson superconducting tunnel junctions in YBa2Cu3O7−δ directly patterned with a focused helium ion beam. *Nat. Nanotechnol.* **2015**, *10*, 598−602.
(28) Jijin, Y.; David, C. F.; Lewis, A. S.; Colin, A. S.; Jason, H.; Zheng, R.; Lu-Chang, Q.; Adam, R. H. Rapid and precise scanning helium ion microscope milling of solid-state nanopores for biomolecule detection. *Nanotechnology* **2011**, *22*, No. 285310.
(29) Emmrich, D.; Beyer, A.; Nadzeyka, A.; Bauerdick, S.; Meyer, J. C.; Kotakoski, J.; Gölzhäuser, A. Nanopore fabrication and characterization by helium ion microscopy. *Appl. Phys. Lett.* **2016**, *108*, No. 163103.
(30) Cai, J.; Zhu, Z.; Alkemade, P. F. A.; van Veldhoven, E.; Wang, Q.; Ge, H.; Rodrigues, S. P.; Cai, W.; Li, W.-D. 3D Volumetric Energy Deposition of Focused Helium Ion Beam Lithography: Visualization, Modeling, and Applications in Nanofabrication. *Adv. Mater. Interfaces* **2018**, *5*, No. 1800203.
(31) Stanford, M. G.; Mahady, K.; Lewis, B. B.; Fowlkes, J. D.; Tan, S.; Livengood, R.; Magel, G. A.; Moore, T. M.; Rack, P. D. Laser-Assisted Focused He+ Ion Beam Induced Etching with and without XeF2 Gas Assist. *ACS Appl. Mater. Interfaces* **2016**, *8*, 29155−29162.
(32) Livengood, R.; Tan, S.; Greenzweig, Y.; Notte, J.; McVey, S. Subsurface damage from helium ions as a function of dose, beam energy, and dose rate. *J. Vac. Sci. Technol. B* **2009**, *27*, 3244−3249.
(33) Livengood, R. H.; Greenzweig, Y.; Liang, T.; Grumski, M. Helium ion microscope invasiveness and imaging study for semiconductor applications. *J. Vac. Sci. Technol. B* **2007**, *25*, 2547−2552.
(34) Novoselov, K. S.; Geim, A. K.; Morozov, S. V.; Jiang, D.; Zhang, Y.; Dubonos, S. V.; Grigorieva, I. V.; Firsov, A. A. Electric field effect in atomically thin carbon films. *Science* **2004**, *306*, 666−669.
(35) Wagner, K.; Cheng, P.; Vezenov, D. Noncontact Method for Calibration of Lateral Forces in Scanning Force Microscopy. *Langmuir* **2011**, *27*, 4635−4644.
(36) Shearer, C. J.; Slattery, A. D.; Stapleton, A. J.; Shapter, J. G.; Gibson, C. T. Accurate thickness measurement of graphene. *Nanotechnology* **2016**, *27*, No. 125704.
(37) Liu, S. W.; Wang, H. P.; Xu, Q.; Ma, T. B.; Yu, G.; Zhang, C. H.; Geng, D. C.; Yu, Z. W.; Zhang, S. G.; Wang, W. Z.; Hu, Y. Z.; Wang, H.; Luo, J. B. Robust microscale superlubricity under high contact pressure enabled by graphene-coated microsphere. *Nat. Commun.* **2017**, *8*, No. 14029.
(38) Yuan, C. C.; Zhang, D.; Gan, Y. Invited Review Article: Tip modification methods for tip-enhanced Raman spectroscopy (TERS) and colloidal probe technique: A 10 year update (2006-2016) review. *Rev. Sci. Instrum.* **2017**, *88*, No. 031101.
(39) Kim, C. S.; Hobbs, R. G.; Agarwal, A.; Yang, Y.; Manfrinato, V. R.; Short, M. P.; Li, J.; Berggren, K. K. Focused-helium-ion-beam blow forming of nanostructures: radiation damage and nanofabrication. *Nanotechnology* **2020**, *31*, No. 045302.

https://dx.doi.org/10.1021/acs.langmuir.0c00923
Langmuir 2020, 36, 7861−7867